Astron. Astrophys. 310, 173–180 (1996)

ASTRONOMY AND ASTROPHYSICS

Rotational modulation and flares on RS Canum Venaticorum and BY Draconis stars

XIX. Simultaneous IUE, ROSAT, VLA, and visual observations of TY Pyxidis*

J.E. Neff[1,**,***], **I. Pagano**[2,***], **M. Rodonò**[2,***], **A. Brown**[3,†], **R.C. Dempsey**[3,‡], **D.C. Fox**[3,§], **and J.L. Linsky**[3]

[1] Department of Astronomy & Astrophysics, The Pennsylvania State University, 525 Davey Laboratory, University Park, PA 16802, USA
e-mail: jneff@astro.psu.edu

[2] Istituto di Astronomia, Università degli Studi, and Osservatorio Astrofisico di Catania, Città Universitaria, Viale Andrea Doria 6, I-95125 Catania, Italy

[3] Joint Institute for Laboratory Astrophysics, Campus Box 440, University of Colorado, Boulder, CO 80309–0440, USA

Received 30 May 1995 / Accepted 28 September 1995

Abstract. In November 1990, we observed the eclipsing binary system TY Pyxidis with the IUE satellite simultaneously with the ROSAT All-Sky Survey. The IUE and ROSAT/WFC observations covered the 3.2-day period of this system continuously, while the ROSAT/PSPC coverage was limited to 2.26 days. We also observed TY Pyx with the VLA for a total of 22 hours throughout this period, and we obtained simultaneous visual photometry and spectroscopy. We compare the rotational and eclipse modulation of the ultraviolet line fluxes and line profiles with the x-ray, extreme-ultraviolet, radio, and visual-light variability. We present the multi-wavelength light curves, and we compare the high-resolution Mg II k profiles with the simultaneously obtained Ca II K profiles. Although the visual light curve suggests the presence of large photospheric spots, no rotational modulation is evident in the ultraviolet, x-ray, and radio flux. This suggests that the outer atmosphere is more uniformly covered with magnetic activity than the photosphere. The rare absence of large flux variations permits us to study an RS CVn system with large intrinsic ultraviolet, x-ray, and radio fluxes but without complications introduced by large active regions or flares. Until now, among the extensively monitored RS CVn systems, only the long-period Capella has shown such a constant radiative output.

Key words: stars: activity – stars: chromospheres – stars: coronae – stars: individual: HD 77137 – stars: starspots

1. Introduction

The ROSAT All-Sky Survey from August 1990 through January 1991 provided a unique opportunity to study the variability of the emission arising from stellar coronae. Each x-ray source was "scanned" for about 30 seconds every 96 minutes for two days, or longer for sources at high ecliptic latitudes. The ROSAT Wide-Field Camera (WFC) extreme-ultraviolet survey, with its wider field of view, provided longer scans over a longer timeline. Thus, the ROSAT All-Sky Survey yielded uniformly-sampled x-ray and extreme-ultraviolet (XUV) light curves of bright sources for 2 to 5 days each. Because RS CVn-type stars having rotational periods in this range are among the brightest x-ray sources (Rosner et al. 1985) and generally show rotationally-modulated light variability, we planned to study one of these sources simultaneously over a wide range of wavelengths simultaneous with the ROSAT all-sky survey.

Phase-dependent variability (*rotational modulation*) of the emission from these systems can be used to probe the spatial structure of their atmospheres. Procedures for infering the spatial structure of *photospheres* are described by Vogt et al. (1987). These procedures exploit the correspondence between wavelength on a rotationally-broadened line profile and location on the stellar surface. Neff et al. (1989) describe a similar procedure to map the structure of stellar *chromospheres* using ultravi-

Send offprint requests to: J.E. Neff

* Table 1 is available only in electronic form at the CDS via anonymous ftp 130.79.128.5

** Visiting Astronomer, National Solar Observatory, National Optical Astronomy Observatories, which is operated by AURA, Inc. under cooperative agreement with the National Science Foundation.

*** Guest Investigator with the International Ultraviolet Explorer satellite, which is sponsored and operated by the National Aeronautics and Space Administration, by the the Science Research Council of the United Kingdom, and by the European Space Agency.

† Visiting Scientist, Rutherford Appleton Laboratory.

‡ Now at Computer Sciences Corporation and Space Telescope Science Institute

§ Now at the Harvard/Smithsonian Center for Astrophysics

olet emission line profiles. Both of these techniques rely on the rotational modulation of line profiles. They can provide detailed maps, but only of the photosphere and lower chromosphere.

At present, the only way to probe the spatial structure of stellar *coronae* is through x-ray and XUV light curves. Prior to the ROSAT All-Sky Survey, such light curves had been obtained for only two stars. Walter et al. (1983) demonstrated the application of eclipse mapping to stellar coronae, using EINSTEIN observations of AR Lacertae. White et al. (1990) and Culhane et al. (1990) used full-orbit x-ray light curves from EXOSAT to provide a more complete picture of the coronae of AR Lacertae and TY Pyxidis, respectively. Ottmann et al. (1993) used ROSAT data to obtain x-ray maps of the corona of AR Lacertae.

The spatial structure of the stellar coronae, chromospheres, and photospheres very likely all are controlled by magnetic fields. By conducting spectroscopic observations *simultaneously* in the visible, ultraviolet, and x-ray bands, i.e. by studing simultaneously the photospheric, chromospheric, and coronal emissions, we effectively can map the magnetically active regions in three dimensions. We arranged for spectroscopic and photometric observations of TY Pyxidis at all possible wavelengths during the entire period when the star was being scanned by ROSAT and observable by IUE within the ROSAT-IUE All Sky Survey (RIASS) program (a preliminary report was given by Neff et al. 1992). An initial paper (Fox et al. 1994) dealt with the time-averaged characteristics in the context of a larger x-ray, ultraviolet, and radio survey. In this paper, we concentrate on the multiwavelength and rotational-modulation aspects.

2. Observations and data reduction

TY Pyxidis (HD 77137; m_v=6.87) is composed of two nearly identical ($M/M_\odot$ = 1.22 and 1.20), slightly-evolved G5 IV stars, which we presume rotate synchronously with their orbital period (P_{orb}=P_{rot}=3.1986 d; $v \sin i$=30 km s^{-1} for each component). Their radii are almost equal and the orbital inclination is i=88°, so mutual partial eclipses occur. Accurate determinations of the system parameters are given by Andersen et al. (1981), and the x-ray coronae were mapped by Culhane et al. (1990). Unless otherwise specified, we use the system parameters compiled by Strassmeier et al. (1993). We use the ephemeris Φ = HJD 2443548.6695 + 3.198584 E, whereby the primary eclipse of the brighter but slightly less massive (secondary) star occurs at Φ = 0.0.

2.1. The IUE observations

We observed TY Pyx continuously with IUE during the period 10–13 November 1990 throughout the system's 3.2 day orbital (and rotational) cycle. The observing dates were chosen to bracket the ROSAT All-Sky Survey window. We obtained 33 LWP high-dispersion (2000–3200 Å; $\Delta\lambda \sim 0.24$ Å) and 11 SWP low-dispersion (1200–2000 Å; $\Delta\lambda \sim 6$ Å) spectra. We interleaved the observations to acquire maximum time resolution of the LWP spectra, but the SWP images typically contain three separate 30–40 minute exposures obtained over a 4–5 hour time interval.

The Fine Error Sensor (FES) on IUE can be used as a photometer provided that proper attention is placed on locating the star exactly at the "reference point" and a correction is applied for the focus. We obtained accurate FES magnitudes between each exposure. We present the entire FES data set in Table 1 (which is available only in electronic form from the CDS via anonymous ftp to 130.79.128.5), including the offsets from the actual reference point and the focus step. We used the FES counts-to-magnitude conversion given by Perez (1991), which includes a preliminary focus correction.

The IUE spectra were independently reduced at Penn State and at the Catania ASTRONET node. The RDAF software distributed by the IUE project at NASA/GSFC were used to calibrate the data. We measured the low-dispersion line fluxes using gaussian fits to the emission lines plus a quadratic fit to the background. Our fitting routines (described in Walter et al. 1987) allow multiple gaussians, so blended lines can be fit accurately by constraining the line width to be the instrumental resolution. While the absolute flux values derived at Penn State and Catania differed by as much as 20% in the faintest and the blended lines, the relative fluxes at all phases for a given line were consistent between the two sets of measurements to better than a 5%. For consistency with the Fox et al. (1994) paper, we list in Table 2 the fluxes measured at Catania.

The high-resolution Mg II k (2795.5 Å) line profiles were analyzed using the procedures described by Neff et al. (1989). Gaussian profiles were fitted to the two stellar emission components and to the interstellar absorption line. The interstellar line was constrained to have instrumental width. Because the instrumental width is known and because the wavelength and equivalent width of the interstellar absorption should remain constant, the interstellar line provides a constant-velocity reference on the spectrum. The resulting parameters from these fits are given in Table 3.

2.2. The ROSAT PSPC and WFC observations

During each 96 minute orbit, ROSAT scanned a great circle of ecliptic longitude, covering the entire sky in six months. For a more complete description of the All Sky Survey, see Cruddace et al. (1989). The PSPC is sensitive to x-rays in the energy range 0.1–2.4 keV. For a description of the instrument, see Trümper (1983) and Pfeffermann et al. (1987). TY Pyx fell within the 2° diameter field of view of the PSPC for approximately 30 sec of each orbit over ~2.26 days, i.e., about 30 independent 30-sec measurements were obtained over ~2.26 days covering about 70% of the TY Pyx orbital period.

The WFC, with a 5° field of view, observed TY Pyx for ~80 sec during each orbit for ~7 days, i.e. covering more than 2 complete TY Pyx orbits. The observations were done alternatively in two filters, S1A and S2A, with bandpasses of 0.08–0.18 keV (65–155 Å) and 0.06–0.11 keV (110–195 Å), respectively. The WFC data for TY Pyx were analysed at the Rutherford Appleton Laboratory (RAL) using the standard WFC anal-

Table 2. Measured ultraviolet emission line fluxes[a]

Φ	C III	N V	O I	C II	Si IV	C IV	He II	C I	Si II	Al III	Si III
–0.03	c	1.8	1.2	3.9	1.2	8.2	2.2	1.6	2.2	1.2	1.2
0.03	1.7	1.7	1.5	3.3	2.3	9.1	2.1	2.5	2.6	1.0	0.8
0.11	1.5	1.7	2.4	3.9	2.1	9.0	2.0	2.2	3.1	0.8	0.7
0.20	0.9	1.4	1.9	3.2	2.0	7.8	1.6	1.7	2.4	0.8	0.9
0.29	0.5	1.7	1.9	4.3	2.4	7.5	1.7	2.4	2.8	0.6	1.1
0.40	2.7	1.6	1.8	3.4	1.5	7.7	2.0	2.1	2.4	0.5	0.8
0.50	2.0	1.3	1.2	2.7	1.6	7.3	1.4	1.6	2.5	0.8	0.9
0.59	1.4	2.0	1.5	3.9	3.6	10.0	1.6	2.6	2.6	c	c
0.70	1.5	1.2	1.4	3.6	2.1	8.4	1.7	2.4	2.5	1.0	0.8
0.81	1.5	1.3	1.6	3.5	1.9	8.8	1.5	1.5	2.1	c	0.8
0.92	1.3	1.4	1.9	4.0	2.4	10.2	2.0	2.1	2.6	0.6	1.3
mean[b]	1.41	1.54	1.80	3.73	2.25	8.68	1.76	2.12	2.56	0.72	0.91
σ^b	0.59	0.24	0.29	0.34	0.58	0.96	0.19	0.35	0.28	0.17	0.20

[a]Units are 10^{-13} erg s^{-1} cm^{-2}.
[b]Calculated from out-of-eclipse spectra only.
[c]Not measureable.
Line identification: C III: 1175 Å; N V: 1239-1243 Å; O I: 1302-1305-1306 Å; C II: 1334-1336 Å; Si IV: 1394-1403 Å; C IV: 1548-1551 Å; He II: 1640 Å blended with Fe II; C I: 1658 Å + O III] 1658-1661 Å; Si II: 1808-1817 Å; Al III: 1855 Åblended with Fe III; Si III]: 1892 Å + S I 1900 Å + C III] 1909 Å

ysis package ASTERIX, which is part of the STARLINK system, and a number of customized routines. An event list was created for the region containing TY Pyx by extracting events from the survey data stream. Maps of this region were made and time series of the source and background signals calculated. The only source present in a 1° diameter circle was TY Pyx itself. The mean count rates were estimated by calculating the radial distribution of counts about the source position to estimate the backgound counts lying beneath the source (see Kellett et al. 1995 for method). This method uses the average background signal representative of the epoch that the star was observed but does include background signal that may refer to times several days earlier or later than the stellar observation. The WFC sensitivity declined steadily during the survey, and in November 1990 the S1 and S2 responses had declined by factors of 0.787 and 0.888 respectively compared to the start of the Survey. The observed count rates were corrected for this effect.

For both the PSPC and the WFC, we use only count rates in this paper. Absolute flux calibrations and further details of the analysis techniques for the x-ray and XUV observations are given by Dempsey et al. (1993) and Wood et al. (1995), respectively.

2.3. The VLA observations

Supporting VLA observations were obtained over a total of 22 hours on 9-12 November. The full data set and a description of their calibration and analysis can be found in Fox et al. (1994). In this paper, we use only the 3.6-cm-band data, because it provides the most complete radio light curve.

2.4. Ground-based observations

The Ca II K line is formed only slightly deeper in the chromosphere than the Mg II k line, so it should be similarly useful for chromospheric imaging. The advantage of higher signal-to-noise Ca II K observations (relative to the IUE Mg II k spectra) is offset by the much higher level of the photospheric continuum at 3934 Å. Furthermore, continuous observations for several days, free of clouds and a day/night duty cycle, are possible only from space. In order to investigate the practicality of ground-based chromospheric imaging, we obtained high-resolution Ca II K spectra simultaneously with the Mg II k spectra.

Using the stellar spectrograph at the McMath–Pierce telescope (National Solar Observatory), we obtained two spectra per night during 10–15 November 1990. We used the Milton Roy grating with 830 grooves per millimeter in 3rd order, the 150 mm lens, the 5-slice image slicer, and the TI #4 800×800 CCD. This configuration yielded a spectral resolution $\lambda/\Delta\lambda$ of ~25,000 and a spectral coverage of ~65 Å. Our exposure times (see Table 4) were typically 2.5 hours, resulting in a signal-to-noise (per pixel) of >150 in the continuum and >50 at the base of the Ca II K (3934 Å) absorption core. These spectra of the Ca II H and K lines are comparable in resolution to the IUE spectra of the Mg II h and k lines, but they have much higher signal-to-noise.

Table 3. Measured parameters of Mg II k lines

Φ	λ_S^a	W_S^b	F_S^c	λ_P^a	W_P^b	F_P^c	λ_{ism}^a	EW^d
–0.037	2795.971	.79	29.2	2796.450	.80	35.4	2795.757	.22
–0.013	2796.027	.80	17.9	2796.357	.85	36.1	2795.818	.22
0.012	2796.471	.84	16.6	2796.206	.84	34.1	2795.833	.20
0.036	2796.483	.84	33.7	2795.966	.83	33.8	2795.803	.25
0.064	2796.642	.87	37.3	2795.844	.75	33.2	2795.777	.31
0.091	2796.727	.86	35.0	2795.689	.87	32.0	2795.749	.25
0.121	2796.834	.86	34.9	2795.608	.71	33.3	2795.718	.34
0.152	2797.012	.84	33.8	2795.556	.84	35.7	2795.768	.29
0.185	2797.061	.92	33.8	2795.457	.86	32.8	2795.725	.25
0.216	2797.123	.85	34.1	2795.374	.96	34.7	2795.731	.18
0.234	2797.141	.91	35.4	2795.363	.93	31.7	2795.723	.19
0.278	2797.064	.82	34.7	2795.283	.82	34.7	2795.644	.23
0.309	2797.044	.80	32.1	2795.355	.81	34.8	2795.666	.30
0.344	2796.922	.83	30.7	2795.444	.80	37.0	2795.649	.35
0.382	2796.852	.84	31.9	2795.627	.87	30.7	2795.757	.21
0.415	2796.714	.89	33.6	2795.783	.99	34.0	2795.775	.21
0.448	2796.500	.81	33.3	2795.935	.82	32.9	2795.781	.26
0.487	2796.420	.82	32.4	2796.022	.82	19.5	2795.840	.26
0.520	2796.072	.77	34.2	2796.582	.83	19.1	2795.784	.21
0.554	2795.856	.87	30.6	2796.495	.87	36.2	2795.748	.23
0.587	2795.759	.81	34.6	2796.737	.83	35.5	2795.744	.31
0.622	2795.640	.77	34.0	2796.874	.95	38.1	2795.718	.26
0.649	2795.483	.83	32.2	2796.955	.84	34.4	2795.717	.30
0.684	2795.440	.92	38.3	2797.056	.86	36.3	2795.715	.32
0.722	2795.407	.84	31.2	2797.168	.88	33.8	2795.743	.19
0.756	2795.398	.84	36.9	2797.178	.92	37.2	2795.733	.20
0.791	2795.484	.89	37.6	2797.186	.85	37.1	2795.777	.29
0.825	2795.472	.86	37.6	2797.094	.86	34.1	2795.728	.32
0.858	2795.495	.83	33.0	2796.898	.92	34.5	2795.680	.28
0.891	2795.574	.84	31.7	2796.736	.90	35.9	2795.708	.26
0.924	2795.895	.87	35.0	2796.710	.81	30.9	2795.753	.20
0.949	2795.897	.86	32.6	2796.468	.80	32.8	2795.696	.21
0.979	2795.953	.82	25.4	2796.368	.82	31.4	2795.750	.29
Mean^e	—	.85	34.1	—	.86	34.4	2795.743	.25
σ^e	—	.03	2.1	—	.06	1.9	0.046	.05

[a] Measured gaussian centroid wavelength, in Å. S=Secondary, P=Primary.
[b] FWHM of gaussian fit, in Å. S=Secondary, P=Primary.
[c] Integrated gaussian line flux, in 10^{-13} erg s^{-1} cm^{-2}. S=Secondary, P=Primary.
[d] Equivalent width, in Å, of interstellar absorption component.
[e] Calculated from out-of-eclipse spectra only.

3. Results

3.1. The visual light variability

We acquired 73 photometric measurements of TY Pyx with the FES during the period of our IUE observations (Table 1). Because these were obtained uniformly in phase, with no gaps due to clouds or to day/night duty cycle, the resulting light-curve (shown with the eclipse phases removed in the middle panel of Fig. 1) is extremely valuable. The minimum of the photometric wave occurred slightly after secondary eclipse. Assuming that the observed light modulation is due to dark starspots distributed on one of the stars (they could be on either star, or even on both stars), we have used an improved version of the two-spot model code developed at Catania (see Rodonò et al. 1986) to determine the general spot distribution on the photosphere. The algorithm assumes circular spots of equal temperature. The input parameters are the inclination of the rotation axis, the spot and photosphere temperatures, the ratio between the two stars' luminosities, and the limb darkening coefficient. The outputs are the longitude, latitude, and radius of each spot.

Table 4. Ca II H and K spectra obtained at the NSO McMath–Pierce telescope

DATE	UT Start	Exp min	$\Phi^a_{\rm mid}$	λ_S Å	W_S Å	F^b_S	λ_P Å	W_P Å	F^b_P
10 Nov 90	10:37	150	0.059	3934.65	0.71	0.16	3933.73	0.72	0.15
11 Nov 90	10:21	150	0.368	3935.06	0.65	0.13	3933.18	0.76	0.20
12 Nov 90	10:33	150	0.683	3933.03	0.74	0.17	3935.38	0.76	0.20
13 Nov 90	10:08	165	0.992	—	—	0.32[c]	—	—	—
14 Nov 90	10:06	155	1.303	3935.37	0.71	0.14	3932.96	0.80	0.21
			mean:	—	0.70	0.15	—	0.76	0.19
			σ:	—	0.03	0.02	—	0.03	0.02

[a] Phases are computed using the ephemeris HJD 2443548.6695 + 3.198584 E.
[b] Arbitrary flux units; continuum normalized. S=Secondary, P=Primary.
[c] Total flux from both stars.

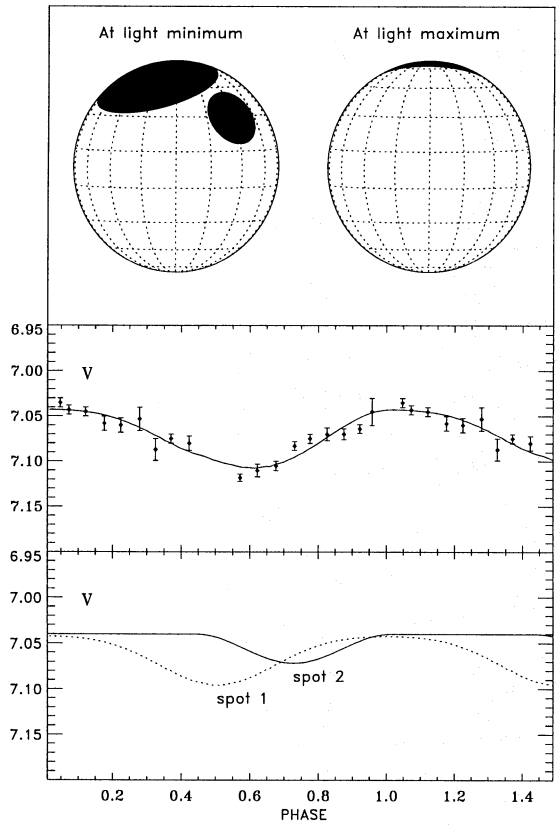

Fig. 1. Results of spot model computations. *Upper panel*: Spot configuration at light minimum and maximum. The larger spot is at latitude 69° and longitude 182° and has a radius of 37°. The smaller spot is at latitude 30° and longitude 262° and has a radius of 16°. *Middle panel*: Comparison between IUE FES observations (filled circles) and the computed light curve (continuous line). The eclipse phases have been removed to better illustrate the spot-induced variation, and several FES measurements are averaged for each datum. *Bottom panel*: The contribution of the individual spots to the computed light curve.

The temperature of the unspotted photosphere (T_{star}) was assumed to be 5400 K, as interpolated from the temperatures for a G5 V and a G5 III star (Schmidt-Kaler 1982); the adopted temperature is in agreement with the estimate by Andersen et al. (1981). The spot temperature (T_{spot}) was assumed 1100 K cooler than the photosphere (Eaton 1992). The luminosity ratio of the two stars in the V-band, L_{hot}/L_{cool}=0.91, was derived from the absolute magnitudes in Strassmeier et al. (1993). The linear darkening coefficient (μ=0.59) was taken from Wade & Rucinski (1985) for a surface gravity log g=4.09 (Andersen & Popper 1975). The maximum luminosity of our light curve (V=7.04) was assumed as the immaculate level, so that the spot configuration resulting from our code accounts only for the observed modulation. Thus, we do not account for either a uniform distribution or polar spots, which would always be visible. We cannot compare the V magnitudes at light maximum with the values given in the literature, because the FES-V magnitudes could be affected by some unknown offset of the magnitude scale.

The best-fit to the observed light curve from our spot model and the spot configuration at light maximum and minimum are shown in Fig. 1. The ratio between the spot area and the total visible surface area was 12%. The larger spotted area reaches its maximum visibility very close to Φ = 0.5, when the primary star is eclipsed, suggesting that it lies on the cooler secondary star.

3.2. Variability of ultraviolet emission line fluxes

Representative chromospheric and transition region fluxes, derived by summing the flux in several appropriate emission lines, are shown in Fig. 2. Only the Mg II k line clearly showed variation due to eclipses. The eclipses were barely visible in the far-ultraviolet (SWP) lines, because the eclipse duration ($\Delta\Phi$ ~0.07) is comparable to the total time it took to acquire a multiply-exposed SWP image. The only significant out-of-eclipse flux variation in any of the ultraviolet lines is the brief rise in the transition region lines at Φ = 0.59.

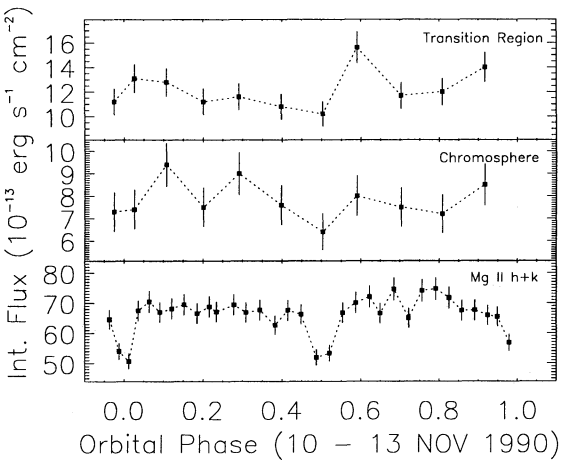

Fig. 2. The integrated emission line fluxes from C IV, Si IV, and N V are summed to represent the transition region (top panel), and the chromospheric emission level (middle panel) is the sum of C II, Si II, and O I. The total Mg II k flux is shown in the bottom panel. The higher time resolution of the Mg II data permit us to resolve the eclipses, and there was a short-lived enhancement of the transition region at $\Phi = 0.59$, but there was no significant rotational modulation.

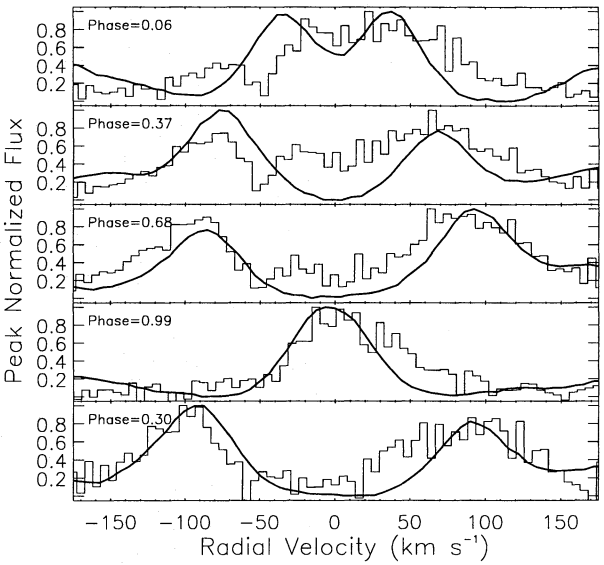

Fig. 3. A comparison of the Ca II K (heavy solid lines) and Mg II k (histograms) profiles. The top 3 are compared with the Mg II k spectrum obtained simultaneously, while the last 2 are compared with spectra obtained at the same phase but one cycle earlier. All profiles are normalized to the peak intensity in the displayed bandpass. Zero velocity corresponds to the predicted photospheric velocity (i.e. the γ velocity).

3.3. Variation of Mg II k and Ca II K line profiles

The Mg II k emission lines from the two stars showed constant and equal flux and FWHM outside of eclipse (see Table 3). Thus, there was no significant difference in the surface distribution of the chromospheric emission between opposite hemispheres, as has been frequently seen on the G2 IV + K0 IV system AR Lac (Neff 1992).

The measured Mg II k centroid velocities of both stars were systematically offset by +15 km s^{-1} with respect to the expected (i.e., photospheric) velocity curve. The measured interstellar medium Mg II k absorption wavelength line velocity was 23.0 km s^{-1}. If we assume that the true interstellar medium velocity for this line of sight is 17.1 km s^{-1}, as predicted using the formula of Crutcher (1982), then there must be a systematic error in the IUE wavelength scale of 5.9 km s^{-1} plus a systematic redshift of 9.1 km s^{-1} in the emitting material in the outer atmospheres of both stars in TY Pyx. More likely, the entire difference is due to a systematic error in the IUE wavelength scale, which would imply that the radial velocity of the interstellar matter in the direction of TY Pyx is only 8 km s^{-1}.

Both the Ca II K and Mg II k profiles were symmetric about their line centers, implying that the chromospheric emission was uniformly-distributed across the stellar surfaces. Although the Mg II k lines from the two stars are identical, the Ca II K emission lines are not. The Ca II K emission from the primary star was 25% brighter and its FWHM 10% greater than the secondary star (see Table 4). In Fig. 3 we compare the Ca II K profiles with the Mg II k profiles observed at the same phases. The Ca II K data have much higher signal-to-noise, but were obtained at only five phases, only three of which were simultaneous with the IUE observations.

The best-fit velocity using the out-of-eclipse Ca II K emission lines, relative to the photospheric velocity, is -2.1 ± 2.1 km s^{-1}. This confirms that the systematic Mg II offset is due to an error in the IUE wavelength scale rather than a systematic flow in the chromosphere.

3.4. X-ray and XUV variability

The PSPC count rates are shown in Fig. 4. The inital and final two scans, when TY Pyx was near the edge of the field of view, have been omitted. The data are consistent with a constant source with a count rate of 1.9 ± 0.4 s^{-1} (see Dempsey et al. 1995).

Because of the poor signal-to-noise ratio of the WFC data, we have rebinned them into "daily" averages for each filter (Fig. 4). The mean count rate for all seven days, taken together, was 0.03 ± 0.04 s^{-1}. In order for us to detect variability, the XUV flux would have to change by a factor of two or more, so the observed lack of variability is not a very useful constraint.

3.5. Radio flux variability

In this paper we consider only the variability of the 3.6 cm flux; Fox et al. (1994) present entire data set. Only the last 3 days, which were taken simultaneously with the ROSAT PSPC coverage, are shown in Fig. 4. During the first two of these days, the 3.6 cm flux was constant (1.43 and 1.54 mJy). On the third day it was about 3 times brighter (4.48 mJy) than the previous two days and over twice as bright as it was one orbital cycle earlier. This variation likely results from a flare that occurred any

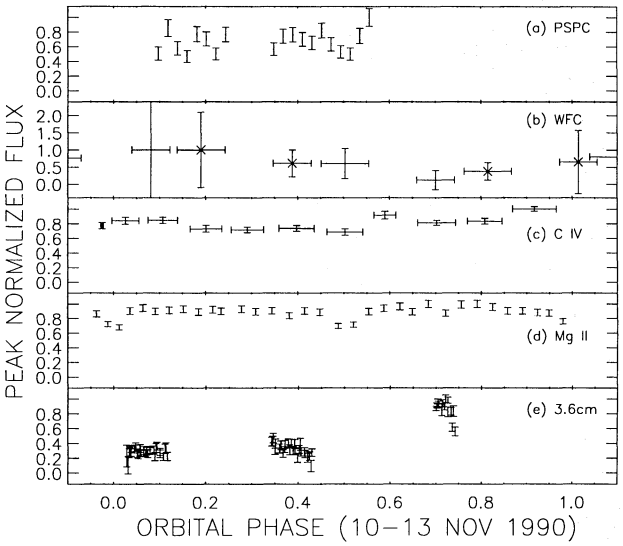

Fig. 4a–e. The multiwavelength light curve for TY Pyx. All plots are normalized to their peak flux value. **a** PSPC x-ray count rates. **b** WFC extreme-ultraviolet count rates. These data are in the same peak-normalized form, but the scale is expanded to fit the error bars. The points marked with an X are taken through the S2 filter, and the rest with the S1 filter. **c** C IV (1550 Å) fluxes. The error bars were determined from gaussian fits with different quadratic background estimates. **d** Mg II k (2795.5 Å) fluxes, with 10% error bars. **e** 3.6 cm radio fluxes for TY Pyx, averaged over 10 minute intervals, with 1σ uncertainties.

time between $\Phi = 0.43$ and $\Phi = 0.70$ or to intrinsic variability, rather than from rotational modulation.

4. Discussion

4.1. Comparison of variability at different atmospheric levels

In addition to the eclipse variability, TY Pyx exhibits the RS CVn characteristic "wave" in its visual light curve. As shown in Fig. 1, the wave was present in November 1990. Its peak-to-peak amplitude 0.07 mag, which corresponds to a total visual flux variation of only ~7%, was consistent with past epochs (Strassmeier et al. 1993). If there were a direct spatial correspondence between starspots and magnetic active regions in the outer atmosphere, we might expect the chromospheric and coronal emission to vary in anti-phase with the visual light (for the most dramatic example of this phenomenon, see Rodonò et al. 1987). We did not see any such variation from TY Pyx in November 1990 (Fig. 4).

4.2. A possible flare

The transition region emission and radio fluxes were higher from phase $\Phi = 0.6$–0.9 than from phase $\Phi = 0.1$–0.4. An enhancement of C IV flux of at least a factor of 1.3 times occurred during the exposure centered at $\Phi = 0.59$. If this enhancement were due to a flare, the peak enhancement would have been much higher. The Mg II k fluxes, obtained with finer phase sampling, do not show any evidence for a flare, but enhancement of the transition region lines is normally far larger and it decays more rapidly than for the chromospheric lines (see Neff 1991). The PSPC count rate in the last two bins was 50% (=3σ) higher than its mean brightness for the rest of the period, suggestive of a coronal flare occuring at the same time. Unfortunately, our PSPC coverage ended immediately after this, and presumably before the peak intensity of the flare. The 3.6 cm flux at $\Phi \sim 0.7$ was three times higher than the flux from the other hemisphere, and it was twice the level seen on the previous cycle. The radio, far-ultraviolet, and x-ray data taken together suggest that coronal flare occurred between $\Phi = 0.57$ and $\Phi = 0.61$ and then decayed over the next 24 hours. This phase interval included the hemisphere with the largest spot concentration.

4.3. The volume emission measure distribution

The absence of rotational modulation of emission fluxes presents us with the rare opportunity to derive a very accurate and complete model for the mean structure of the outer atmosphere of TY Pyx. The complete volume emission measure (VEM) distribution, constructed using fluxes averaged over the rotational cycle of TY Pyx, from the lower chromosphere into the corona is presented in Fig. 5. When deriving values for the VEM we made no correction for obscuration effects due to the stellar disk. Such effects are likely to have a different values for different atmospheric regions. If both the transition region and corona are compact, then the plotted values of the VEM should be a factor of 2 larger. We used the IUE line fluxes given in Tables 2 and 3 and the mean ROSAT PSPC (1.9 ct s^{-1}) and WFC count rates (S1: 0.018 ct s^{-1}, S2: 0.048 ct s^{-1}). We used the new Napiwotzki et al. (1993) PSPC calibration with 77% higher soft x-ray response. Without this calibration we would not get a common solution between the PSPC and the WFC data. We have consistent values of the VEM at roughly log T = 6.3 and 7.3, where the S1, S2, and PSPC curves overlap. The Dempsey 2-temperature solution is shown as asterisks in Fig. 5. Clearly there is better agreement with the PSPC data at higher rather than lower temperatures. Our solutions suggest significant VEM at slightly hotter temperatures than the Dempsey et al. (1993) values.

5. Summary

We simultaneously observed diagnostic emissions from the corona, transition region, chromosphere, and photosphere of TY Pyx. Although the photospheric emission varied in a fashion suggesting an asymmetric distribution of starspots, the chromospheric, transition region, and coronal emission fluxes were essentially constant except during the eclipses and a possible flare. Within the accuracy of our measurements, the Mg II k and Ca II K lines show symmetric profiles about their expected wavelengths, and the Mg II k profiles from the two stars are identical. The lack of rotational modulation of line fluxes and the observed symmetry of the line profiles imply an overall uniformity of the emission from the outer atmosphere of TY Pyx. We were

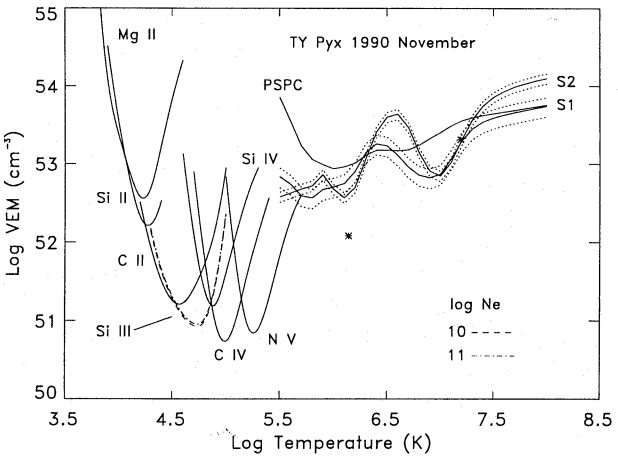

Fig. 5. The complete emission measure distribution from the lower chromosphere into the corona. The dotted lines show the 1 sigma errors for the WFC curves – the PSPC eror is too small to be differentiated from the plotted locus. The dashed curves shown for different values of electron density refer to the Si III] VEM loci. Asterisks show the VEM results of Dempsey et al. (1993).

therefore able to use the time-averaged fluxes obtained over an entire rotational cycle to construct a volume emission measure distribution that allows us to probe the mean atmospheric structure over the temperature range from the lower chromosphere up through the corona.

Acknowledgements. We would like to express our gratitude to those who assisted in obtaining the data in the core campaign, especially to J. Bonnell and R. Pitts at IUE (NASA/GSFC). This work was supported by NASA grant NAGW-2603 to the Pennsylvania State University, by Interagency Transfer W-17,772 from NASA to the National Institute of Standards and Technology, and by NASA grants NAG5-82, NAG5-1792, and NAG5-1797 to the University of Colorado. The Italian coauthors acknowledge support for stellar activity research at Catania University and Astrophysical Observatory by the Ministero dell'Università e della Ricerca Scientifica e Tecnologica (MURST), the Consiglio Nazionale delle Ricerche: Gruppo Nazionale di Astronomia (CNR: GNA) and the Agenzia Spaziale Italiana (ASI). AB thanks the staff of Rutherford Appleton Laboratory for their hospitality and support. RCD would like to thank Prof. Trümper and the staff of the Max-Planck-Institut für extraterrestrische Physik for their hospitality during his stay in Garching bei München. The ROSAT project is supported by the German Bundesministerium für Forschung und Technologie (BMFT/DARA) and by the Max-Planck-Society.

References

Andersen J., Clausen J.V., Nordström B., Reipurth B., 1981, A&A 101, 7
Andersen J., Popper D.M., 1975, A&A 39, 131
Cruddace R.G., Hasinger G., Trümper J., et al., 1989, Experimental Astron. 1, 365
Crutcher R.M., 1982, ApJ 254, 82
Culhane J.L., White N.E., Shafer R.A., Parmer A.N., 1990, MNRAS 243, 424
Dempsey R.C., Linsky J.L., Fleming T.A., Schmitt J.H.M.M., 1993, ApJS 86, 599
Dempsey R.C., Linsky J.L., Schmitt J.H.M.M., Kürster M., 1995, ApJS, submitted
Eaton J.A., 1992, In: Byrne P.B., Mullan, D.J. (eds.) Surface Inhomogeneities on Late-Type Stars. Springer-Verlag, Berlin, p. 15
Fox D.C., Linsky J.L., Veale, A., Dempsey R.C., et al., 1994, A&A 284, 91
Kellett B.J., Bromage G.E., Brown A., et al., 1995, ApJ 438, 364
Napiwotzki R., Barstow M.A., Fleming T., et al., 1993, A&A 278, 478
Neff J.E., 1991, Mem. Soc. Astron. Ital. 62, 291
Neff J.E., 1992, In: Byrne P.B., Mullan, D.J. (eds.) Surface Inhomogeneities on Late-Type Stars. Springer-Verlag, Berlin, p. 54
Neff J.E., Pagano I., Rodonò M., Bonnell J., 1992, In: Giampapa M., Bookbinder J. (eds.) Cool Stars, Stellar Systems, and the Sun. ASP Conf. Series 26, p. 52
Neff J.E., Walter F.M., Rodonò M., Linsky J.L., 1989, A&A 215, 79
Ottmann R., Schmitt J.H.M.M., Kürster M., 1993, ApJ 413, 710
Perez M., 1991, NASA IUE Newsletter 45, p. 19
Pfeffermann E., Briel U.G., Hippmann H., et al., 1987, In: Koch E.-E., Schmahl G. (eds.) Soft X-Ray Optics and Technology. Proc. SPIE 733, 519
Rodonò M., Cutispoto G., Pazzani V., et al., 1986, A&A 165, 135
Rodonò M., Byrne P.B., Neff J.E., et al., 1987, A&A 176, 267
Rosner R., Golub L., Vaiana G.S., 1985, ARA&A 23, 413
Schmidt-Kaler, T.H., 1982, Physical parameters of the stars. In: Schaifers K., Voigt H.H. (eds.) Landolt-Bornstein New Series, Volume 2b, Astronomy and Astrophysics – Stars and Star Clusters. Springer-Verlag, Berlin
Strassmeier K.G., Hall D.S., Fekel F.C., Scheck M., 1993, A&AS 100, 173
Trümper J., 1983, Adv. Space Res. 2, 241
Vogt S.S., Penrod G.D., Hatzes A.P., 1987, ApJ 321, 496
Wade R.A., Rucinski S.M., 1985, A&AS 60, 471
Walter F.M., Gibson D.M., Basri G.S., 1983, ApJ 267, 665
Walter F.M., Neff J.E., Gibson D.M., et al., 1987, A&A 186, 241
Wood B.E., Brown A., Linsky J.L., 1995, ApJ 438, 350
White N.E., Shafer R.A., Parmer A.N., Culhane J.L., 1990, ApJ 350, 776

This article was processed by the author using Springer-Verlag LaTeX A&A style file version 3.